International Journal of Heat and Mass Transfer 55 (2012) 5709–5721

Contents lists available at SciVerse ScienceDirect

International Journal of Heat and Mass Transfer

journal homepage: www.elsevier.com/locate/ijhmt

Analysis of biofilm growth in the presence of osmotic pressure and temperature effects

Uzair Ahmed, Kambiz Vafai *

Department of Mechanical Engineering, University of California, Riverside 92521, United States

ARTICLE INFO

Article history:
Received 13 March 2012
Received in revised form 16 May 2012
Accepted 22 May 2012
Available online 25 June 2012

Keywords:
Biofilm
Temperature effects
Osmotic pressure

ABSTRACT

Transient mass transfer in a diffusion–reaction biofilm with a moving boundary was investigated analytically. The analysis incorporates both the diffusion processes into the biofilm as well as the reaction processes that lead to the expansion of the system. For first and second order reaction terms, the biofilm synthesis as a function of time was presented. The temporal development of the biomass was found to be in very good agreement with numerical results. The effects of osmotic pressure and temperature were also investigated and it was found that osmotic pressure plays a significant role in first order reactions but the temperature dependence is primarily found in the reaction kinetics and does not significantly influence osmotic pressure effects.

1. Introduction

Biofilms, a structured community of microorganisms encapsulated within a self-developed polymeric matrix and adherent to a living or inert surface, can be valuable tools or severe impediments in engineered systems. The effects of biofilms on natural and engineered systems can be desirable, undesirable, or disastrous depending on the location of biofilm accumulation and their microbial community structures [1]. For example, desirable accumulation of biofilms is on trickling filters in wastewater treatment. An undesirable accumulation is in cooling towers and heat exchangers. A disastrous accumulation is on tampons or implantable prosthetic devices. With respect to the last example, the former can cause serious illness and death, while the latter requires surgical removal [1]. The National Institute of Health estimates that biofilms are involved in over 80% of human infections [2–5]. Irrespective of the location, function, and structure of the biofilm, there is a common desire to understand and control formation, growth, and removal.

Biofilms are investigated through both experimentation and theoretical modeling. Experimentation gives rise to new observations which in turn motivates mechanistic representations of the phenomena. Mathematical models have become widely accepted as a crucial tool in linking all of the components and processes that encompass these complex microbial ecosystems [6]. Analytical models cannot predict distributions of different bacteria, conversion of multiple substrates, or complex biofilm structure but they can be useful in analyzing the effects of various parameters.

There are two methods that have been historically used to provide mechanistic representations of biofilm: as distinct particles or as a continuum body. Distinct particles approach discusses the behavior of individual cells and the phenomena that occur at that scale. In models with a discrete description of particulate components, individual cells and particles are displaced according to empirical rules that mimic advective or diffusive flux [7]. In principle, individual-based models can also describe cell-based transport phenomena such as bacterial motility and chemotaxis [8].

Modeling as a continuum body is the traditional method to solve mass conservation equations. Instead of discussing the behavior of the individual cells, this approach provides the average concentration of the components. Transport of the particulate components occurs when the solid matrix of the biofilm expands or contracts as a result of bacterial growth, bacterial decay, and EPS production [7]. The movement of these components can be represented by advective flux, diffusive flux, or both [8–16].

Shafahi and Vafai [4,5] and Wanner and Gujer [17] developed a, homogenous multicomponent model to serve as a tool for investigating basic microbial interactions. The work was later expanded to include the particulate and dissolved phases of biofilm. Shafahi and Vafai [4] presented a comprehensive investigation of biofilm formation in both a macro scale and micro scale by developing a set of multispecies biofilm models with complex reaction kinetics that capture the key physical attributes of previous models that exist in literature. These models were applied to a network of spheres that approximate a porous matrix to investigate changes in porosity and permeability during biofilm formation. Alpkvist et al. [18] developed a hybrid, continuum-particle, model to investigate the temporal development of biofilm structure in two and

* Corresponding author. Tel./fax: +1 951 827 2135.
E-mail address: vafai@engr.ucr.edu (K. Vafai).

0017-9310/$ - see front matter © 2012 Elsevier Ltd. All rights reserved.
http://dx.doi.org/10.1016/j.ijheatmasstransfer.2012.05.066

Nomenclature

C	concentration (g/m^3)
D	diffusion coefficient (m^2/day)
k	reaction coefficient (m^3/g-day)
j	flux (g/m^2-day)
k_B	Boltzmann constant (g-m^3/Kelvin-day)
k_S	saturation constant (g/m^3)
T	temperature (Kelvin)
t	time (day)
u	expansion velocity (m/day)
x	spatial coordinate (m)

Subscripts

b	bulk
i	microbial index
H	high
j	nutrient index
L	low
max	maximum
op	osmotic pressure
ss	steady state
$trans$	transient

Greek symbols

δ	biofilm thickness (m)
ε	volume fraction
η	viscosity (g/m-day)
κ	permeability (m^2)
λ	biomass detachment coefficient (1/m-day)
μ	specific growth rate (1/day)
ν	volume occupied by one monomer (m^3)
ρ	density (g/m^3)
ρ^*	total effective density (g/m^3)
σ	rate of flocculation (m/day)
χ_1	flory interaction parameter
ψ	osmotic pressure (g/m-day^2)

three spatial dimensions. This model attempted to explain the consolidation effects that lead to biofilm shrinkage. Cogan and Keener [19] investigated biofilms as a polymeric matrix using statistical thermodynamics by applying Flory–Huggins solution theory. They modeled the biofilm as a biological gel composed of EPS and water. The bacteria were enmeshed within the network and were the producers of the polymer. As the solvent was absorbed or repelled, osmotic pressure gradients caused the polymer to swell or contract.

A common bacterium used to study biofilm growth is *Pseudomonas aeruginosa* (PA). It has been shown to have anywhere from highly irregular shapes to flat and homogenous, depending on growth conditions [7]. The continuous layer assumption is the most accurate for cases with sufficient nutrients [4]. PA is to found be non-toxic in its planktonic form. However, once it becomes a biofilm, it becomes highly toxic. Biofilm/EPS formation does not occur until the colony is of sufficient size to overwhelm the immune system. Prior to this, it cannot be detected by the immune system.

The effect of heat transfer on biofilm has rarely been analyzed in the open literature. The only studies in literature that have considered the effects of temperature on biofilms were carried out at the macro scale level to indicate how biofilms reduce efficiencies by resisting heat transfer. However the direct effect of temperature on biofilm synthesis has not been investigated.

Bott and Pinheiro [20] have shown experimentally the effects of varying bulk fluid temperatures on the growth of a biofilm predominantly composed of *Escherichia coli* (*E. coli*). They had shown that even a small increase in temperature increases the biofilm thickness significantly. They further noted that the optimum temperature for growth of the predominant bacteria in the biofilm was only a few degrees higher than the temperature at which the experiment was conducted. Else et al. [21] investigated the effects of relative humidity and temperature on the biofilm formation at a nuclear waste repository. It was found that reductions in relative humidity and escalations in temperature hindered biofilm synthesis. They found that temperature played a key role in that EPS production did not occur at extreme temperatures but did so at intermediary temperatures for the bacteria they investigated.

The purpose of this work is to evaluate the effects of osmotic pressure, and indirectly environmental temperature, as a primary contributor/inhibitor to biofilm growth. First, an analytical solution of biofilm growth is presented and compared to numerical and experimental results to determine its accuracy. Finally, the contribution of pressure and temperature will be established.

2. Theory and governing equations

A biofilm model is proposed in which biomass is irreversibly attached to a surface, as shown in Fig. 1, and is beginning to expand. The following assumptions are invoked in solving the problem.

(1) Homogenous, one dimensional growth.
(2) Bulk concentration remains constant at the biofilm-bulk fluid interface due to minimal resistance across the boundary layer [4].
(3) Single nutrient species.
(4) No flux through the surface.

Based on these assumptions and the physical processes, a set of governing equations was obtained as shown in Shafahi and Vafai [4,5].

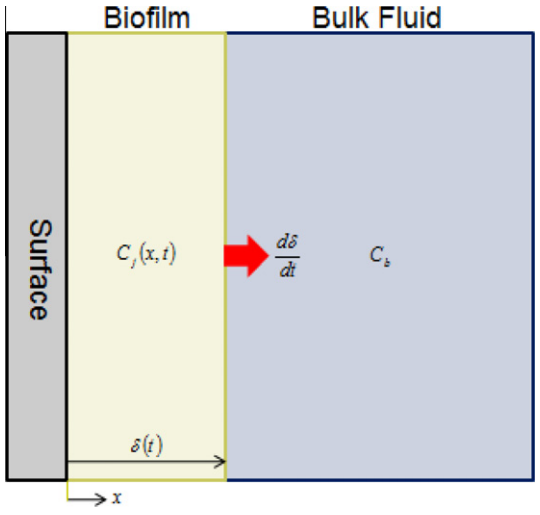

Fig. 1. Model schematic for present work.

2.1. Particulate phase

Problems of mass transfer involving reactions can become complex since the boundary between the biofilm and bulk fluid moves as nutrients dissolved in the fluid diffuse into the biofilm and are consumed resulting in biofilm development. The location of the moving interface is not known a priori and is usually a result of systems of nonlinear equations with multiple phases and nutrients. Previous methods solve this problem numerically as a result of this nonlinearity. Currently there are no analytical solutions for this problem.

For biofilm growth, movement of the interface is dependent on reaction kinetics and mass transfer, thus a boundary condition for the movement of the interface, otherwise known as the expansion velocity, must be determined.

Conservation of mass for microbes can be represented by

$$\frac{\partial \rho_i}{\partial t} + \nabla \cdot j_i^m = r_i \quad i = 1, \ldots, N_m \tag{1}$$

where ρ_i is microbial density, r_i the reaction rate and j_i the total flux.

Since bulk motion is dominant, the flux can be represented as:

$$j_i^m = \rho_i u \tag{2}$$

where u is the velocity.

Thus, Eq. (1) becomes

$$\frac{\partial \rho_i}{\partial t} + \nabla \cdot (\rho_i u) = r_i \tag{3}$$

If it is assumed that the microbial species are incompressible and ϵ_i is the volume fraction of these species:

$$\rho_i = \varepsilon_i \rho_i^* \tag{4}$$

Thus:

$$\frac{\partial \varepsilon_i}{\partial t} + \nabla \cdot (\varepsilon_i u) = \frac{r_i}{\rho_i^*} \tag{5}$$

Taking the summation over all of the microbes

$$\sum_{i=1}^{2} \frac{\partial \varepsilon_i}{\partial t} + \sum_{i=1}^{2} \nabla \cdot (\varepsilon_i u) = \sum_{i=1}^{2} \frac{r_i}{\rho_i^*} \tag{6}$$

Expanding

$$\frac{\partial}{\partial t} \sum_{i=1}^{2} \varepsilon_i + u \cdot \nabla \left(\sum_{i=1}^{2} \varepsilon_i \right) + (\nabla \cdot u) \sum_{i=1}^{2} \varepsilon_i = \sum_{i=1}^{2} \frac{r_i}{\rho_i^*} \tag{7}$$

Since $\sum_{i=1}^{2} \varepsilon_i = 1$, Eq. (7) reduces to:

$$\nabla \cdot u = \sum_{i=1}^{2} \frac{r_i}{\rho_i^*} \tag{8}$$

Thus, the biofilm expansion velocity can be written as:

$$u = \int_0^{\delta(t)} \sum_{i=1}^{2} \frac{r_i}{\rho_i^*} dx \tag{9}$$

where $\delta(t)$ is the biofilm thickness at time t. Defining

$$\bar{\mu} = \sum_{i=1}^{2} \frac{r_i}{\rho_i^*} \tag{10}$$

The reaction term can be rewritten as a function of growth rates, μ_i, and densities, thus:

$$r_i = \mu_i \rho_i \tag{11}$$

The average net growth rate can be expressed as:

$$\bar{\mu} = \sum_{i=1}^{2} \frac{r_i}{\rho_i^*} = \sum_{i=1}^{2} \mu_i \varepsilon_i \tag{12}$$

The expansion velocity can be rewritten as

$$u = \int_0^{\delta(t)} \bar{\mu} dx \tag{13}$$

Finally, the biofilm expansion velocity can be represented by

$$u = \int_0^{\delta(t)} \sum_{i=1}^{2} \mu_i \varepsilon_i dx \tag{14}$$

2.2. Dissolved phase – pseudo-steady state

Characteristic times for processes within a biofilm system can vary by up to ten orders of magnitude [7]. The timescale for biofilm growth is much larger than the timescale for substrate diffusion. Thus, the diffusion equation for the dissolved phase can be presented by a steady state approximation and is spatially dependent.

$$\frac{d^2 C_j}{dx^2} - \frac{\rho k}{D_j} C_j = 0 \tag{15}$$

where C_j is the nutrient concentration, k is the reaction coefficient for the production of cellular mass, and D_j is the diffusivity of the nutrients with respect to the biofilm.

The boundary conditions can be specified as

$$\left. \frac{\partial C_j}{\partial x} \right|_{x=0} = 0 \tag{16}$$

$$C_j|_{x=\delta(t)} = C_b \tag{17}$$

Eq. (15) can be rewritten as:

$$\frac{\partial^2 C_j}{\partial x^2} - \omega^2 C_j = 0 \tag{18}$$

where $\omega = \sqrt{\frac{\rho k}{D_j}}$

The solution of which can be written as:

$$C_j = C_b \frac{\cosh \omega x}{\cosh \omega \delta} \tag{19}$$

The average net growth rate can be expressed as:

$$\bar{\mu} = \sum_{i=1}^{2} \frac{r_i}{\rho_i^*} = \sum_{i=1}^{2} \mu_i \varepsilon_i = \mu_1 \varepsilon_1 + \mu_2 \varepsilon_2 \tag{20}$$

For first order reaction kinetics, the bacterial growth rate is defined by

$$\mu_1 = k C_j \tag{21}$$

$$\mu_2 = k_2 k C_j \quad [22] \tag{22}$$

where k_2 is a proportionality constant as the production of EPS is associated with cellular growth [22].

The average net growth rate can then be expressed as:

$$\bar{\mu} = \varepsilon_1 k C_j + \varepsilon_2 k_2 k C_j \tag{23}$$

and from Eq. (13), the biofilm expansion velocity can be represented by

$$u_{ss} = (\varepsilon_1 k + \varepsilon_2 k_2 k)\int_0^{\delta(t)} C_j dx \tag{24}$$

$$u_{ss} = (\varepsilon_1 k + \varepsilon_2 k_2 k)\left[\frac{C_b}{\omega}\tanh\omega\delta\right] \tag{25}$$

$$\frac{d\delta}{dt} = (\varepsilon_1 k + \varepsilon_2 k_2 k)\left[\frac{C_b}{\omega}\tanh\omega\delta\right] \tag{26}$$

$$\delta = \frac{1}{\omega}\sinh^{-1}[c_2 e^{(\varepsilon_1 k+\varepsilon_2 k_2 k)C_b t}] \tag{27}$$

Providing a thickness for the initial condition, the biofilm thickness can be written as:

$$\delta(t) = \frac{1}{\omega}\sinh^{-1}[\sinh(\delta_0\omega)e^{(\varepsilon_1 k+\varepsilon_2 k_2 k)C_b t}] \tag{28}$$

2.3. Dissolved phase – transient zeroth order

If transient effects are to be considered for the dissolved phase, approximate methods can be utilized as outlined below.

$$\frac{\partial C_j}{\partial t} - D_j\frac{\partial^2 C_j}{\partial x^2} = -\bar{\mu} \tag{29}$$

If the concentration profile is approximated as follows:

$$C_j = a\frac{1+bx^2}{1+b\delta^2} \tag{30}$$

From the boundary conditions (16) and (17)

$$a = C_b \tag{31}$$

Evaluating Eq. (13), assuming $\bar{\mu}$ is constant

$$\frac{d\delta}{dt} = \bar{\mu}\delta \tag{32}$$

which results:

$$\delta = \delta_o e^{\bar{\mu}t} \tag{33}$$

However, one more condition is required to determine the final coefficient b as the expansion velocity alone is not satisfactory [23]. This extra condition is obtained by utilizing boundary condition (17)

$$@x = \delta(t) \to C_j|_{x=\delta(t)} = C_b \therefore \left.\frac{dC_j}{dt}\right|_{x=\delta(t)} = 0 \tag{34}$$

$$\Rightarrow 0 = \frac{\partial C_j}{\partial x}\frac{d\delta}{dt} + \frac{\partial C_j}{\partial t} \tag{35}$$

Using Eqs. (32) and (29) in Eq. (35) results in

$$\bar{\mu} - D_j\frac{\partial^2 C_j}{\partial x^2} = \frac{\partial C_j}{\partial x}\bar{\mu}\delta \quad (@x = \delta) \tag{36}$$

This will serve as the interface condition. Using Eq. (30) in Eq. (36) results in

$$\bar{\mu} - D_j a\frac{2b}{1+b\delta^2} = a\frac{2b\delta}{1+b\delta^2}\bar{\mu}\delta \quad (@x = \delta) \tag{37}$$

Solving for b

$$b = \frac{\bar{\mu}}{\bar{\mu}\delta^2(2a-1) + 2aD_j} \tag{38}$$

Thus, results of the dissolved phase when incorporating transient aspects can be summarized as

$$C_j = a\frac{1+bx^2}{1+b\delta^2}$$

With

$$a = C_b$$

$$b = \frac{\bar{\mu}}{\bar{\mu}\delta^2(2a-1) + 2aD_j}$$

And the biofilm thickness can be written as

$$\delta = \delta_o e^{\bar{\mu}t}$$

2.4. Dissolved phase – transient first order

$$\frac{\partial C_j}{\partial t} - D_j\frac{\partial^2 C_j}{\partial x^2} = -\rho k C_j \tag{39}$$

The growth rate can be specified as

$$\frac{d\delta(t)}{dt} = \int_0^{\delta(t)}\bar{\mu}dx = (\varepsilon_1 k + \varepsilon_2 k_2 k)\int_0^{\delta(t)} C_j dx \tag{40}$$

Using the concentration profile given in Eq. (30) and the boundary conditions (16) and (17), Eq. (40) results in

$$u_{trans} = (\varepsilon_1 k + \varepsilon_2 k_2 k)\int_0^{\delta(t)} a\frac{1+bx^2}{1+b\delta^2}dx \tag{41}$$

$$\frac{d\delta}{dt} = (\varepsilon_1 k + \varepsilon_2 k_2 k)\int_0^{\delta(t)} a\frac{1+bx^2}{1+b\delta^2}dx \tag{42}$$

Define $\xi = (\varepsilon_1 k + \varepsilon_2 k_2 k)$ and evaluating Eq. (42):

$$\frac{d\delta}{dt} = \xi\left[a\frac{\delta + \frac{b}{3}\delta^3}{1+b\delta^2}\right] \tag{43}$$

Utilizing the biofilm growth rate, Eqs. (43) and (39), Eq. (35) results

$$\rho k C_j - D_j\frac{\partial^2 C_j}{\partial x^2} = \xi\frac{\partial C_j}{\partial x}\left[a\frac{\delta + \frac{b}{3}\delta^3}{1+b\delta^2}\right] \quad (@x = \delta) \tag{44}$$

Using the concentration profile given in Eq. (30) in Eq. (44) results in

$$\rho k a - D_j a\frac{2b}{1+b\delta^2} = \xi a\frac{2b\delta}{1+b\delta^2}\left[a\frac{\delta + \frac{b}{3}\delta^3}{1+b\delta^2}\right] \quad (@x = \delta) \tag{45}$$

$$\left(\rho k a\delta^4 - 2D_j a\delta^2 - \frac{2}{3}\xi\delta^4 a^2\right)b^2 + (2\rho k a\delta^2 - 2D_j a - 2\xi a\delta^2 a)b + \rho k a = 0 \tag{46}$$

The above equation enables us to solve for b

$$b = \frac{-(2\rho k a\delta^2 - 2D_j a - 2\xi a\delta^2 a) \pm \sqrt{\left[(2\rho k a\delta^2 - 2D_j a - 2\xi a\delta^2 a)\right]^2 - 4(\rho k a\delta^4 - 2D_j a\delta^2 - \frac{2}{3}\xi\delta^4 a^2)\rho k a}}{2(\rho k a\delta^4 - 2D_j a\delta^2 - \frac{2}{3}\xi\delta^4 a^2)} \tag{47}$$

Thus the results of the dissolved phase with first order reaction kinetics when incorporating transient aspects can be summarized as

$$C_j = a\frac{1+bx^2}{1+b\delta^2}$$

with

$$a = C_b$$

$$b = \frac{-(2\rho k a\delta^2 - 2D_j a - 2\xi a\delta^2 a) \pm \sqrt{\left[(2\rho k a\delta^2 - 2D_j a - 2\xi a\delta^2 a)\right]^2 - 4(\rho k a\delta^4 - 2D_j a\delta^2 - \frac{2}{3}\xi\delta^4 a^2)\rho k a}}{2(\rho k a\delta^4 - 2D_j a\delta^2 - \frac{2}{3}\xi\delta^4 a^2)}$$

and the interface velocity can be written as:

$$\frac{d\delta}{dt} = \xi a\frac{\delta + \frac{b}{3}\delta^3}{1+b\delta^2}$$

where $\xi = (\varepsilon_1 k + \varepsilon_2 k_2 k)$

2.5. Osmotic pressure

Osmotic pressure governs the physical morphology of the biofilm and is dependent on temperature, solvent composition, pH, and ionic concentrations [21]. If the biofilm is modeled as a biological gel consisting of a networked polymer (EPS) and solvent (water), bulk motion is dependent on the swelling of the polymer, which results in generation of this pressure, and can be presented by Darcy's Law:

$$u_{op} = -\frac{\kappa}{\eta}\nabla\psi \tag{48}$$

where κ is the permeability, η the viscosity and ψ the osmotic pressure.

From Flory Huggins Theory [19,24,25], the osmotic pressure is given by:

$$\psi = \frac{k_B T}{3\upsilon_1}\varepsilon_n^2\left(\varepsilon_n - 3\left(\chi_1 - \frac{1}{2}\right)\right) \tag{49}$$

where k_B is the Boltzmann's constant, T temperature, υ the volume occupied by one monomer of network constituent and χ_1 the Flory interaction parameter which measures the strength of interaction between polymer chains.

Assuming a linear temperature profile across the biofilm,

$$u_{op} = -\frac{\kappa}{\eta}\frac{k_B}{3\upsilon_1}\varepsilon_n^2\left(\varepsilon_n - 3\left(\chi_1 - \frac{1}{2}\right)\right)\frac{T_H - T_L}{\delta} \tag{50}$$

Thus, the expansion of the biofilm is now proportional to the temperature gradient.

2.6. Dissolved phase – transient monod with osmotic pressure

$$\frac{\partial C_j}{\partial t} - D_j\frac{\partial^2 C_j}{\partial x^2} = -\rho\mu_{\max}\frac{C_j}{k_s + C_j} \tag{51}$$

where k_s is the half saturation constant and the boundary conditions are given by (16) and (17).

For Monod reaction kinetics, the bacterial growth rate is defined by

$$\mu_1 = \mu_{\max}\frac{C_j}{k_s + C_j} \tag{52}$$

$$\mu_2 = k_2\mu_{\max}\frac{C_j}{k_s + C_j} \tag{53}$$

From Eq. (20), the average net growth rate can be expressed as:

$$\bar{\mu} = \varepsilon_1\mu_{\max}\frac{C_j}{k_s + C_j} + \varepsilon_2 k_2\mu_{\max}\frac{C_j}{k_s + C_j} \tag{54}$$

Using Eq. (13), the biofilm expansion velocity can be represented by

$$\frac{d\delta(t)}{dt} = (\varepsilon_1\mu_{\max} + \varepsilon_2 k_2\mu_{\max})\int_0^{\delta(t)}\frac{C_j}{k_s + C_j}dx \tag{55}$$

As the biomass grows or shrinks, an internal pressure is generated which can be described through Darcy's Law. This pressure gradient can be examined through Flory–Huggins theory in which the system is modeled as a networked polymer and solvent and as a result the pressure within the biofilm is osmotic in nature.

$$\frac{d\delta(t)}{dt} = (\varepsilon_1\mu_{\max} + \varepsilon_2 k_2\mu_{\max})\int_0^{\delta(t)}\frac{C_j}{k_s + C_j}dx = u = -\frac{k}{\eta}\nabla\psi \tag{56}$$

This can be utilized for more complex reaction terms where additional nonlinearities appear in the approximation. Using the concentration profile given in Eq. (30) and the boundary conditions (16) and (17),

$$a = C_b \tag{57}$$

Substituting Eq. (30) into Eq. (56)

$$u_{trans} = (\varepsilon_1\mu_{\max} + \varepsilon_2 k_2\mu_{\max})\int_0^{\delta(t)}\frac{a\frac{1+bx^2}{1+b\delta^2}}{k_s + a\frac{1+bx^2}{1+b\delta^2}}dx \tag{58}$$

$$u_{trans} = (\varepsilon_1\mu_{\max} + \varepsilon_2 k_2\mu_{\max})\left[\delta - \frac{k_s(b\delta^2+1)\tan^{-1}\left(\frac{\sqrt{ab}\delta}{\sqrt{a+b\delta^2 k_s + k_s}}\right)}{\sqrt{ab}\sqrt{a+b\delta^2 k_s + k_s}}\right] \tag{59}$$

To determine the coefficient b, the boundary condition given by Eq. (35) is utilized. Inserting the osmotic pressure from Eq. (56) into Eq. (35) results

$$-\frac{\partial C_j}{\partial t} = \frac{\partial C_j}{\partial x}\left[-\frac{k}{\eta}\nabla\psi\right] \tag{60}$$

In addition, inserting Eq. (51) into the LHS of (60):

$$\rho\mu_{\max}\frac{C_j}{k_s + C_j} - D_j\frac{\partial^2 C_j}{\partial x^2} = \frac{\partial C_j}{\partial x}\left[-\frac{k}{\eta}\nabla\psi\right] \quad (@x = \delta) \tag{61}$$

This will serve as the interface condition

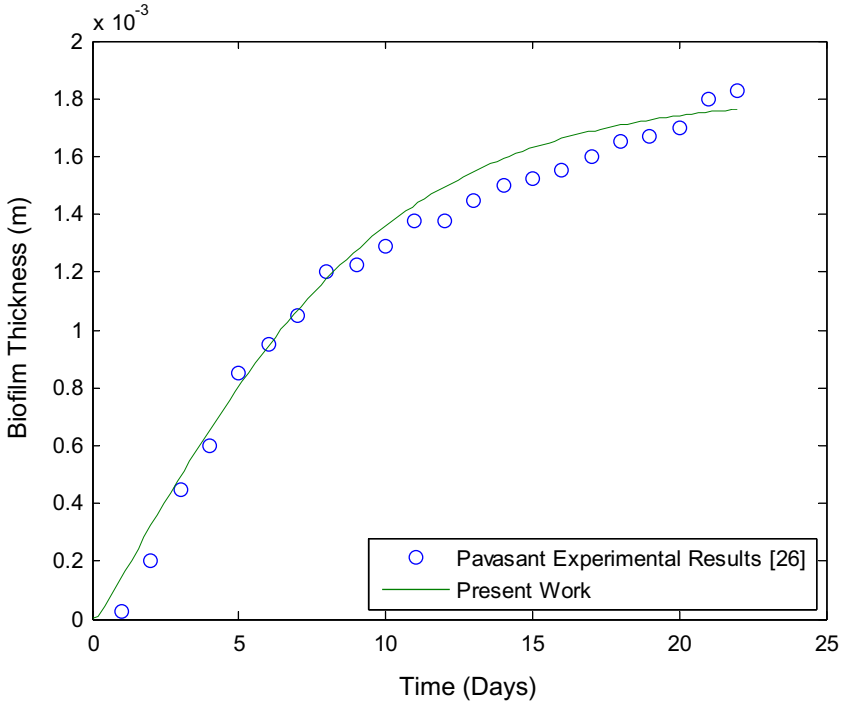

Fig. 2. Comparison of the present work with experimental results from the study on single tube extractive membrane bioreactors (STEMB) conducted by Pavasant et al. [26]. Parameters used: k = 24 g/m^3, k_1 = 0.27, D = 283 × 10^{-6} m^2/day, ρ = 200,000 g/m^3, C_b = 2 g/m^3, δ_0 = 5 × 10^{-6} m, λ = 55 m^{-1} day^{-1}.

Utilizing Eq. (30) in Eq. (61) results:

$$\rho\mu_{\max}\frac{a}{k_s+a} - D_j a\frac{2b}{1+b\delta^2} = a\frac{2b\delta}{1+b\delta^2}\left[-\frac{k}{\eta}\nabla\psi\right] \quad (@x=\delta) \tag{62}$$

$$b = -\frac{\rho\mu_{\max}\frac{a}{k_s+a}}{\delta^2\rho\mu_{\max}\frac{a}{k_s+a} - 2Da + 2a\delta\frac{k}{\eta}\nabla\psi} \tag{63}$$

Thus the results of the dissolved phase when incorporating transient aspects and osmotic pressure can be summarized as

$$C_j(x,t) = a\frac{1+bx^2}{1+b\delta^2}$$

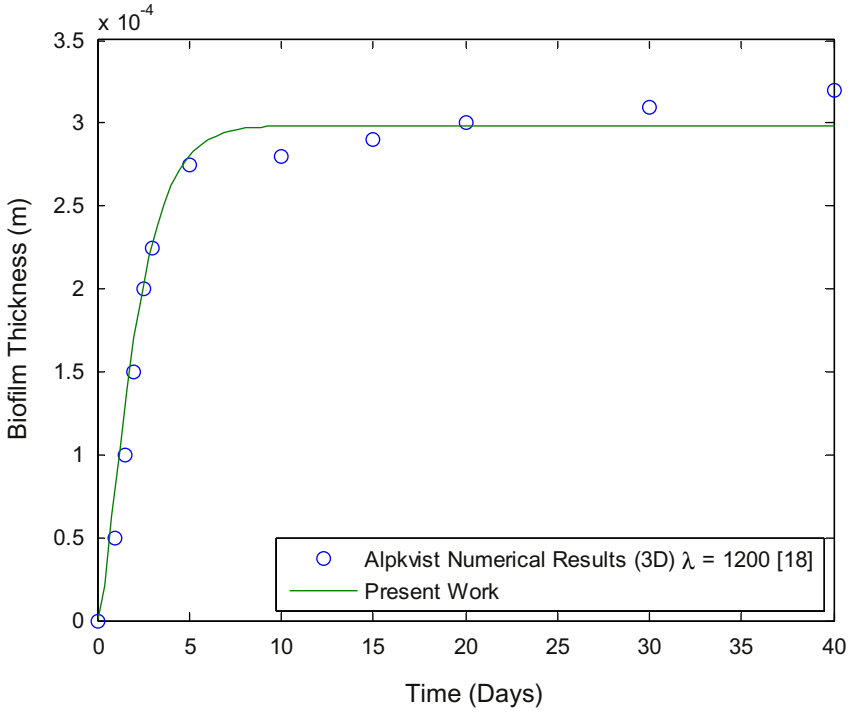

Fig. 3. Comparison of the present work with the averaged thickness from the three dimensional numerical results of Alpkvist et al. [18]. Parameters used: k = 24 g/m^3, k_1 = 0.27, D = 1 × 10^{-4} m^2/day, ρ = 200,000 g/m^3, C_b = 2 g/m^3, δ_0 = 5 × 10^{-6} m, λ = 1200 m^{-1} day^{-1}.

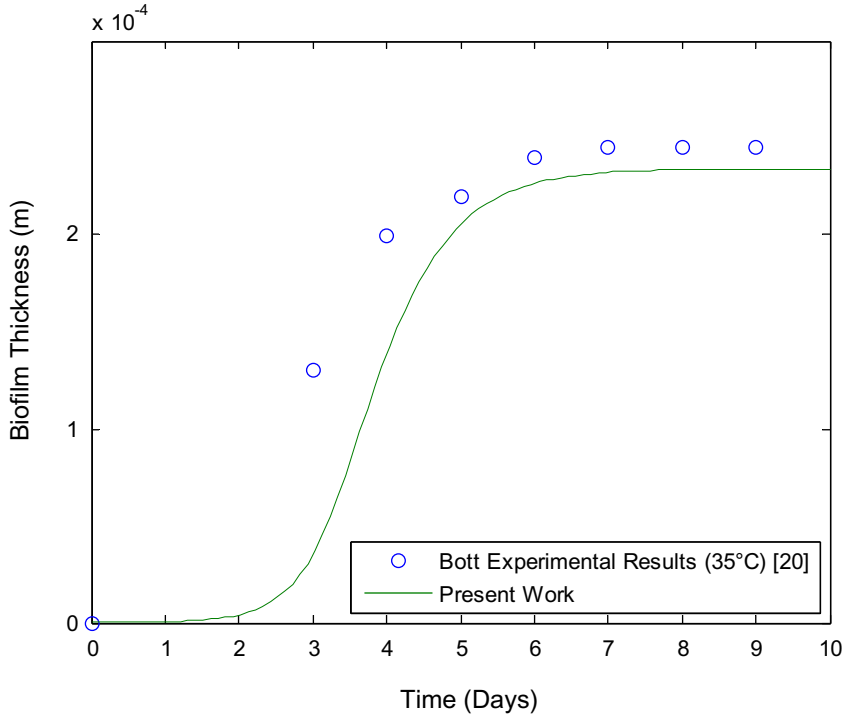

Fig. 4. Comparison of the present work with experimental results from the study on velocity and temperature effects on biological fouling conducted by Bott and Pinheiro [20]. Parameters used: $k = 3$ g/m^3, $k_1 = 0.27$, $D = 83 \times 10^{-6}$ m^2/day, $\rho = 5000$ g/m^3, $C_b = 2$ g/m^3, $\delta_0 = 5 \times 10^{-6}$ m, $\lambda = 3000$ m^{-1} day^{-1}.

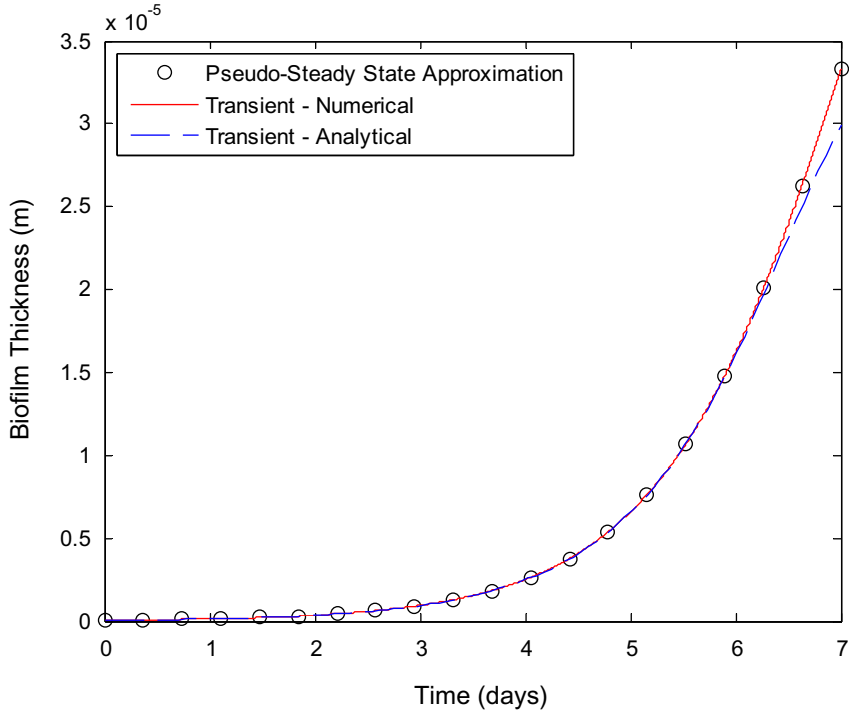

Fig. 5. Validation of the analytical work against the pseudo-steady state approximation and the numerical solution over a period of seven days.

with

$$a = C_b$$

$$b = -\frac{\rho\mu_{\max}\frac{a}{k_s+a}}{\delta^2\rho\mu_{\max}\frac{a}{k_s+a} - 2Da + 2a\delta\frac{k}{\eta}\nabla\psi}$$

and the interface velocity can be written as:

$$\frac{d\delta}{dt} = (\varepsilon_1\mu_{\max} + \varepsilon_2 k_2\mu_{\max})\left[\delta - \frac{k_s(b\delta^2+1)\tan^{-1}\left(\frac{\sqrt{ab}\delta}{\sqrt{a+b\delta^2k_s+k_s}}\right)}{\sqrt{ab}\sqrt{a+b\delta^2k_s+k_s}}\right]$$

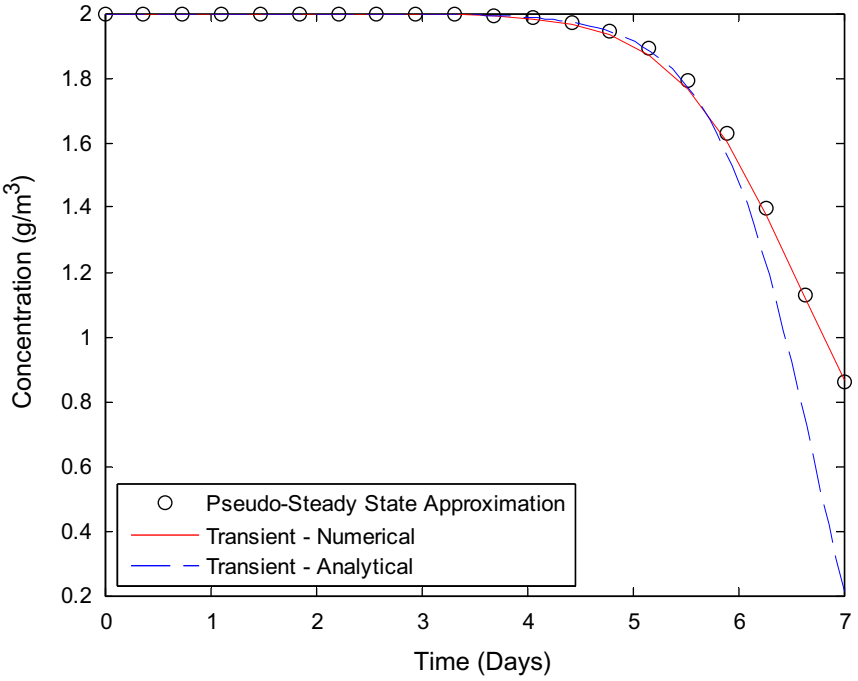

Fig. 6. Comparison of concentration as a function of time at the surface-biofilm interface between the analytical work, pseudo-steady state approximation and the numerical solution.

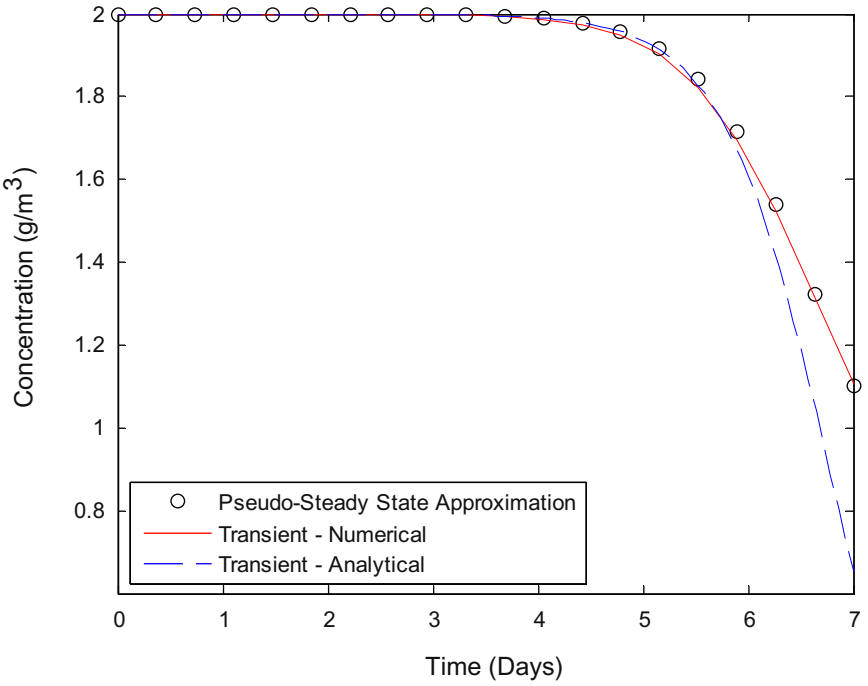

Fig. 7. Comparison of concentration as a function of time at the midpoint between the analytical work, pseudo-steady state approximation and the numerical solution.

2.7. Biofilm shear

To account for biofilm detachment in some situations a dampening coefficient which modifies the interface velocity is introduced [4,17].

$$u|_{x=\delta(t)} = \int_0^{\delta(t)} \bar{\mu} dx + \sigma \tag{64}$$

where σ is a rate of flocculation.

$$\sigma = -\lambda\delta^2 \tag{65}$$

The parameter σ has been empirically shown to be a first-order process with a detachment rate coefficient λ and is proportional to the square of the biofilm thickness. The process can be assumed to occur only at the biofilm surface, equally over the entire biofilm depth, or with different rates at different locations [7].

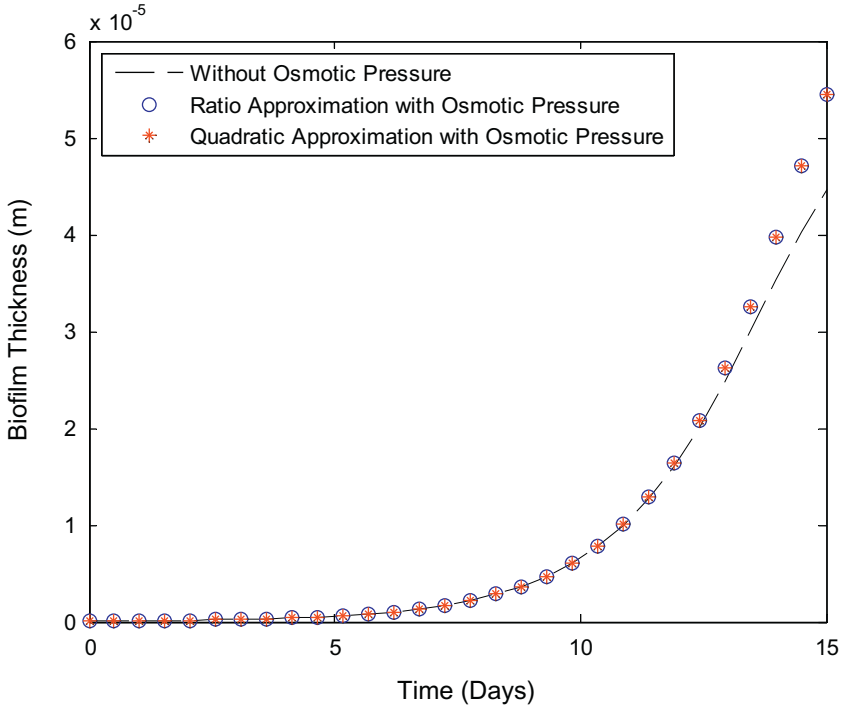

Fig. 8. Comparison of biofilm synthesis for first order reaction kinetics in the cases where osmotic pressure is either included or neglected.

3. Results and discussion

3.1. Comparison with experimental results

In order to validate our analytical results, they were compared to physical systems with similar boundary conditions. Pavasant et al. [26] experimentally investigated single tube extractive membrane bioreactors (STEMB). These systems are used for biotreatment of wastewaters with volatile organic compounds (VOCs), saline wastewater, and for nitrification purposes. Intermediary membranes are used to prevent direct contact between the pollutants and aerated gas (oxygen). The result is counterdiffusion between substrates and a reduction in problems caused by air stripping. The boundary conditions for this system match the ones presented in the current work. The concentration at the boundary between the bulk fluid and biofilm is constant with a no flux

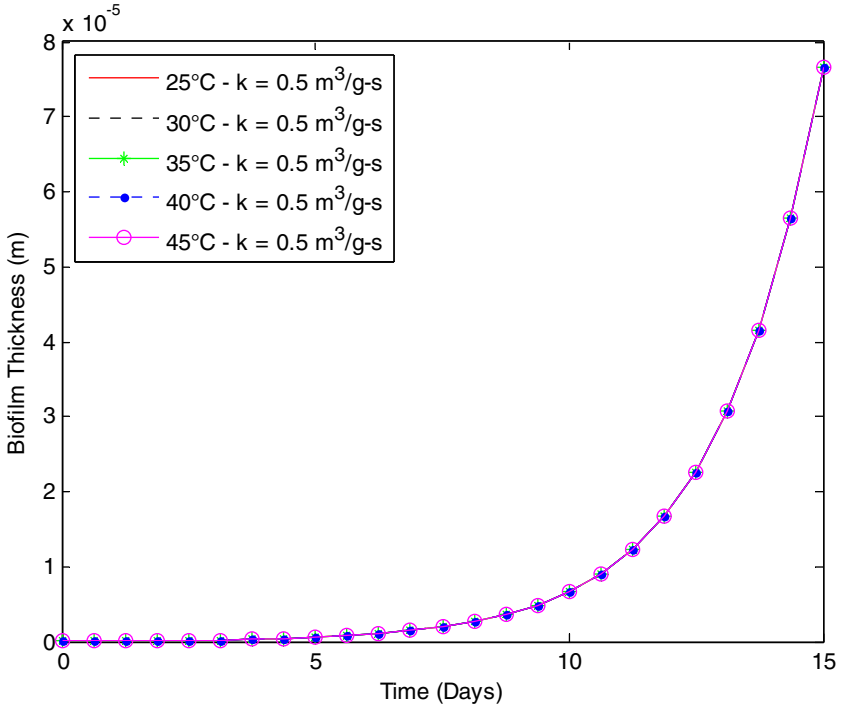

Fig. 9. Variation of temperatures with constant reaction rates for first order reaction kinetics.

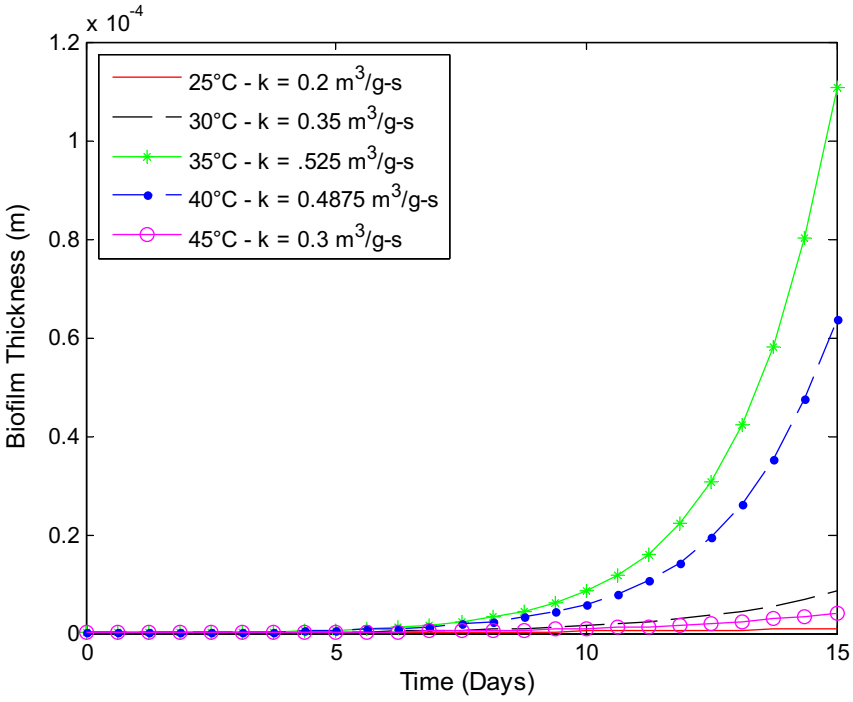

Fig. 10. Variation of temperatures with temperature dependent reaction rates for first order reaction kinetics.

condition at the interface between the biofilm and the membrane. The wastewater solutes do not play a role in the development of the biofilm, only the oxygen does. Thus, a single reaction occurs. Fig. 2 shows how accurately the current work predicts the experimental growth of the system. In order to account for the decay in growth over time, shear was introduced. The current work matches the experimental results well.

Alpkvist et al. [18] developed a hybrid model that combines both the continuum model and the individual particulates. The advantage of creating this hybrid model is that it retains the advantages of both while accurately predicting temporal development. However this model encompasses multiple soluble components within a 3D model. Fig. 3 shows the comparisons of the biofilm thickness based on the current work versus the numerical results of Alpkvist et al. [18]. A detachment rate coefficient of 1200 approximates their numerical thickness well, achieving steady state conditions within 7 days.

Bott and Pinheiro [20] had investigated the effects of temperature and velocity on biological fouling. Fig. 4 illustrates the

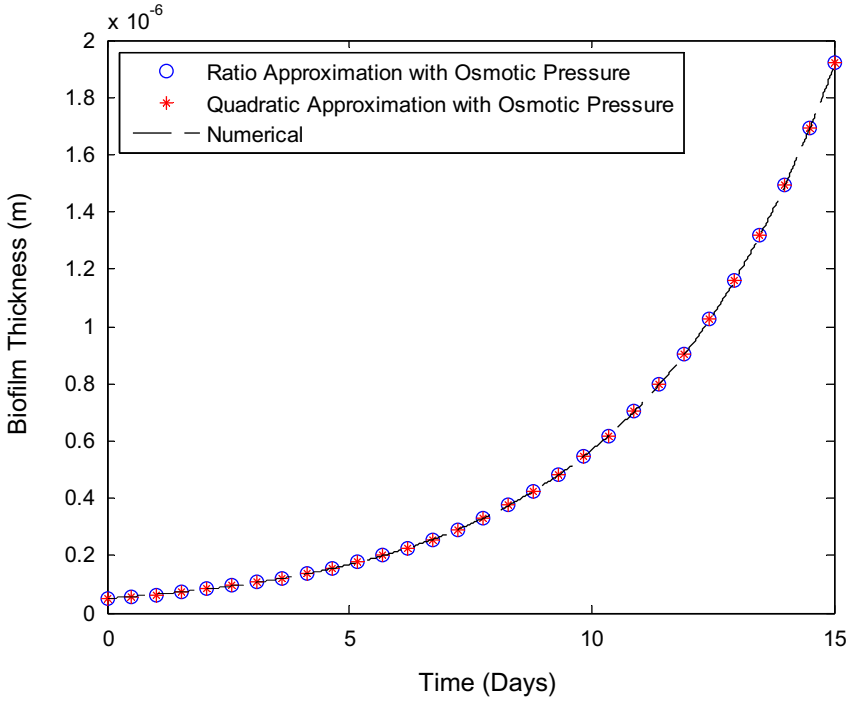

Fig. 11. Comparison of biofilm synthesis for Monod reaction kinetics for the case where osmotic pressure is included with the numerical results where it is neglected.

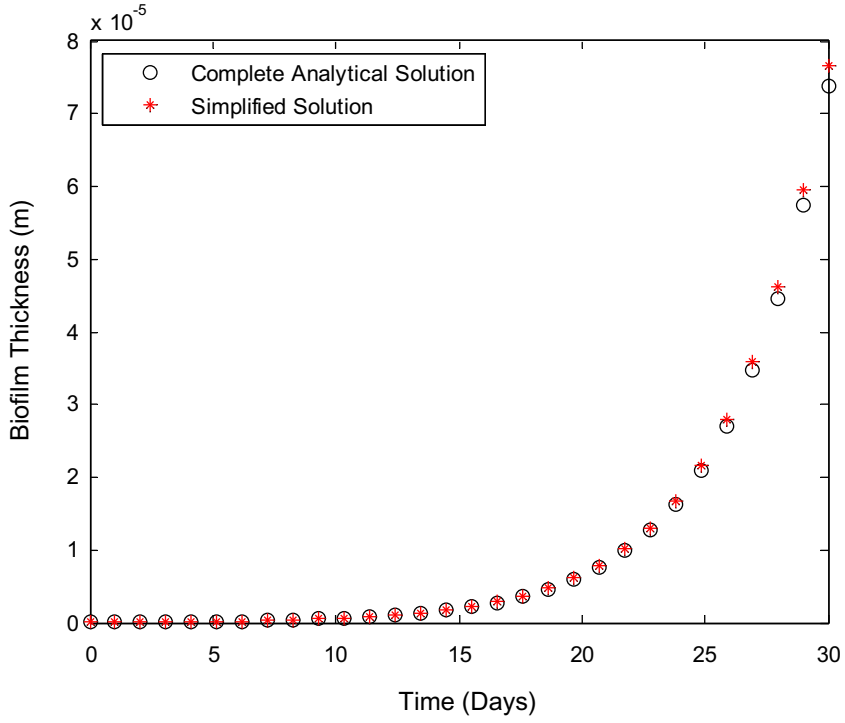

Fig. 12. Comparison between the solution obtained for Monod reaction kinetics with the simplified exponential form represented by Eq. (70).

comparison between their experimental work in a countercurrent heat exchanger and the present work.

3.2. First order reaction kinetics

Two different methods were used to approximate biofilm growth analytically, which were compared with the numerical solution. It was found that for several days the analytical and numerical results match very well. However, as the biofilm thickness increases, the approximation begins to diverge. As such, the analytical results are accurate for the first several days of growth but not representative of the longer term growth of the biofilm. Fig. 5 shows the accuracy of the approximation over seven days.

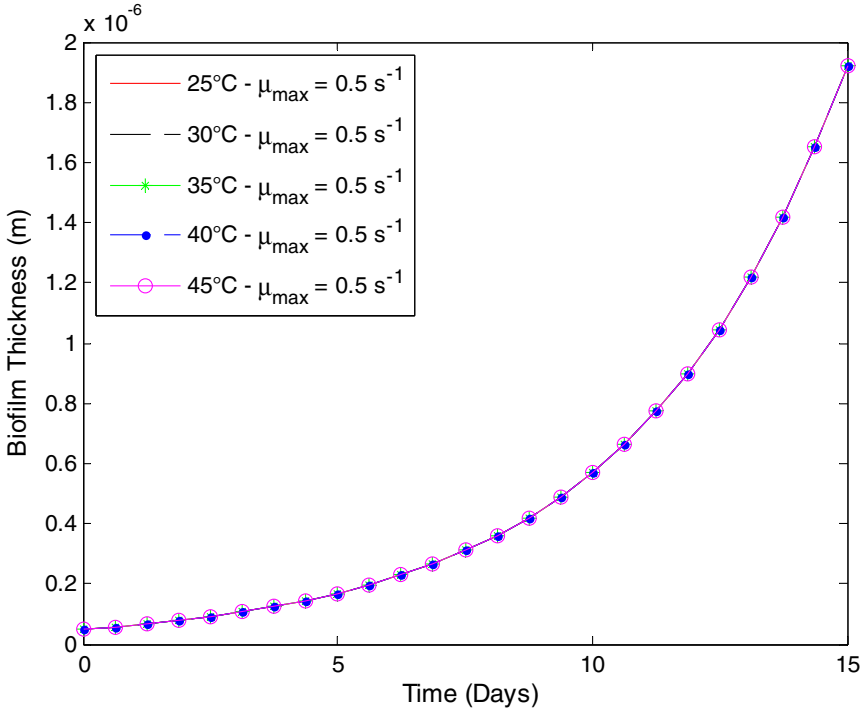

Fig. 13. Variation of temperatures with constant growth rates for Monod reaction kinetics.

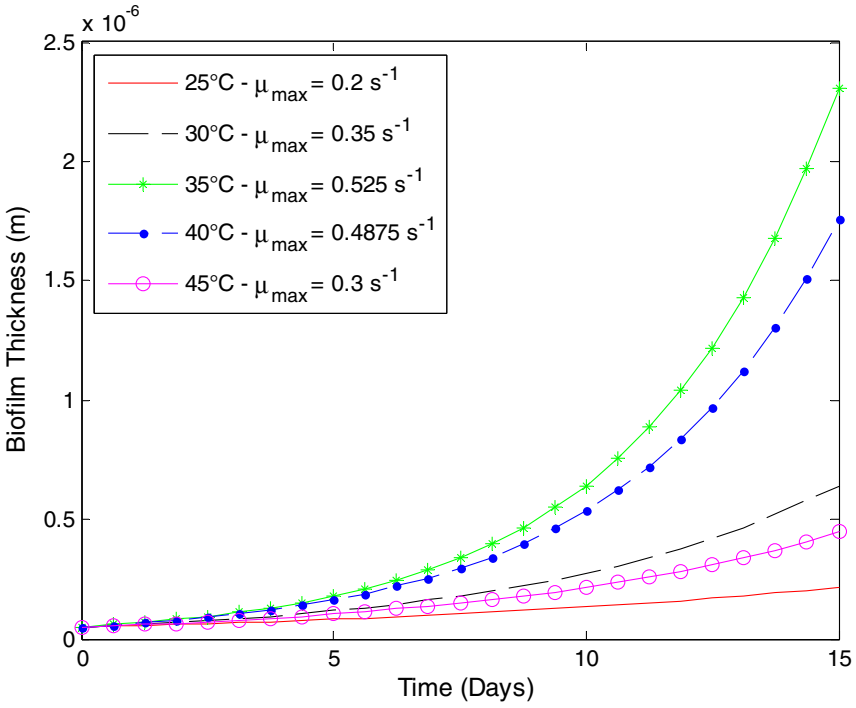

Fig. 14. Variation of temperatures with temperature dependent growth rates for Monod reaction kinetics.

Fig. 6 shows how the concentration at the interface between the surface of attachment and the biofilm. It is clear that at this interface two phenomena occur. The bacteria furthest from the interface will begin dying off and stop contributing to the structural growth as the penetration of dissolved species decreases over time. However as the approximation diverges, it under predicts the concentration of nutrients within the biofilm, hampering growth. Fig. 7 depicts the same problem arising at the midpoint.

However, it should be noted that the pseudo steady approximation matches the numerical results as expected. The time scale for substrate diffusion is much smaller than the timescale for biofilm growth, thus the biofilm growth can be presented by our steady state model. However, the polynomial approximation starts to deviate from the expected curve as time increases.

If the analysis is done similarly to the Monod approximation where osmotic pressure is considered, the results are found to vary only in the coefficient b:

$$b = -\frac{\rho k a}{\delta^2 \rho k a - 2Da + 2a\delta\frac{k}{\eta}\nabla\psi} \tag{66}$$

When the results which include the osmotic pressure are compared to those without, it can be seen, in Fig. 8, that the biomass reaches a higher steady state value when compared to that without osmotic pressure. The quadratic approximation in this figure refers to a third order polynomial of the form

$$C_j(x,t) = a + b(x-\delta) + c(x-\delta)^2 \tag{67}$$

this can also be used to approximate the concentration and the end result matches the presented solution.

As can be seen in Fig. 9, the osmotic pressure alone does not significantly impact the rate of growth. However, temperature can play a role in helping or hindering biofilm growth as can be seen in Fig. 10. Temperature plays a key role in both the diffusion processes as well as the reaction processes since temperature can be considered to be a measure of kinetic energy of a system, a higher temperature leads to a higher average kinetic energy of molecules and higher collision rate. The Arrhenius equations supports the notion that most chemical reaction rates double for every 10 °C increase in temperature. However, beyond a certain temperature, the chemical species are altered (protein denaturation) and the chemical reaction slows down or may stop [27]. Both of these findings are supported by the investigation done by Esener et al. [27] on the relationship between temperature and reaction rate. They used the organism Klebsiella pneumoniae NCTC 418 and cultivated it in a synthetic medium at various temperatures. The dry weights were used to determine the specific growth rates of the organisms. If these results for temperature specific growth rates are used in the current work with osmotic pressure, it can be seen that osmotic pressure has a greater impact at the ends of the temperature spectrum where the reaction rate is lowest [27]. As can be seen in Fig. 10, at 35 °C, the peak reaction rate occurs and biofilm synthesis is maximized.

3.3. Monod reaction kinetics

Inserting the Monod reaction term into the diffusion equation adds another source of nonlinearity in the current problem which necessitates the use of osmotic pressure in the boundary condition for interfacial motion. Otherwise the solution becomes indeterminate. It was found in this case, the approximation matched the numerical solution. Upon further inspection, it was found that

$$\delta \gg \frac{k_s(b\delta^2+1)\tan^{-1}\left(\frac{\sqrt{ab}\delta}{\sqrt{a+b\delta^2k_s+k_s}}\right)}{\sqrt{ab}\sqrt{a+b\delta^2k_s+k_s}} \tag{68}$$

Thus, the expansion velocity could be approximated as

$$\frac{d\delta}{dt} = (\varepsilon_1\mu_{\max} + \varepsilon_2 k_2 \mu_{\max})\delta \tag{69}$$

This leads to a simplified analytical solution

$$\delta = \delta_o e^{(\varepsilon_1\mu_{\max}+\varepsilon_2 k_2\mu_{\max})t} \tag{70}$$

As time progresses, it can be seen in Figs. 11 and 12 there is a slight difference between the numerical and analytical solutions. This is

similar to what was seen in the first order results. This result shows that if osmotic pressure is ignored, the solution is still quite accurate and can be approximated with this simplified solution.

If the effects of temperature and osmotic pressure are also investigated similarly to what was done for the first order reaction terms, it can be seen there is little to no impact from osmotic pressure and significant impact as reaction rates change as a result of temperature (Figs. 13 and 14).

4. Conclusion

Transient mass transfer in a diffusion–reaction system was investigated analytically. The problem presents an interesting nonlinearity in the form of a moving boundary. Our analysis incorporates both the diffusional processes within the biofilm as well as the reaction processes that lead to the expansion of the system for various reaction terms. For zeroth order reaction term, the dissolved phase and particulate phase become decoupled due to the constant growth rate. The results for the first order reaction kinetics show that for periods of the order of several days, the transient analytical results for both the concentration profile and temporal development of the biomass were accurate. Beyond this, there is a deviation from the numerical results. However, the pseudo-steady state approximation accurately represents temporal development of the biofilm. The effects of osmotic pressure were investigated and it was found that in first order reaction kinetics, the inclusion osmotic pressure enhanced biofilm synthesis. This, however, was not the case for Monod reaction kinetics. There was no enhancement or detraction of the biofilm development when compared to the numerical results. Furthermore, the effects of temperature were slightly amplified through the reaction rate as a result of the osmotic pressure. There are few works investigating the effects of temperature on biofilm synthesis. Changes in diffusion and reaction processes due to thermal gradients were investigated in this work for the first time. This is a key issue that needs to be developed further in order to advance the understanding of these complex microbial systems.

References

[1] Z. Lewadowski, H. Beyanal, Fundamentals of Biofilm Research, CRC Press, Florida, 2007.
[2] N.G. Cogan, Effects of persister formation on bacterial response to dosing, J. Theor. Biol. 238 (2006) 694–703.
[3] D. Davies, Understanding biofilm resistance to antimicrobial agents, Nature 2 (2003) 114–122.
[4] M. Shafahi, K. Vafai, Biofilm affected characteristics of porous structures, Int. J. Heat Mass Transfer 52 (2009) 574–581.
[5] M. Shafahi, K. Vafai, Synthesis of biofilm resistance characteristics against antibiotics, Int. J. Heat Mass Transfer 53 (2010) 2943–2950.
[6] B.E. Rittman, Where are we with biofilms now? Where are we going?, Water Sci Technol. 55 (8) (2007) 1–7.
[7] O. Wanner, H. Eberl, E. Morgenroth, D. Noguera, C. Piocioreanu, B. Rittmann, M. Van Loosdrect, Mathematical Modeling of Biofilms, IWA, 2006.
[8] R. Dillon, L. Fauci, D. Gaver, A microscale model of bacterial swimming, chemotaxis and substrate transport, J. Theor. Biol. 177 (4) (1995) 325–340.
[9] B.E. Rittmann, J.A. Manem, Development and experimental evaluation of a steady-state, multispecies biofilm model, Biotechnology 39 (1) (1992) 914–922.
[10] J. Dockery, I. Klapper, Finger formation in biofilm layers, SIAM J. Appl. Math 62 (3) (2001) 853–869.
[11] H.J. Eberl, D.F. Parker, M.C.M. van Loosdrecht, A new deterministic spatio-temporal continuum model for biofilm development, J. of Theor. Med. 3 (2001) 161–175.
[12] O. Wanner, P. Reichert, Mathematical modeling of mixed-culture biofilms, Biotechnology 49 (1996) 172–184.
[13] C. Picioreanu, M.C. van Loosdrecht, J.J. Heijnen, Mathematical modeling of biofilm structure with a hybrid differential-discrete cellular automaton approach, Biotechnol. Bioeng. 58 (1) (1998) 101–116.
[14] J.U. Kreft, C. Picioreanu, J.W. Wimpenny, M.C. van Loosdrecht, Individual-based modeling of biofilms, Microbiology 147 (2001) 2897–2912.
[15] G. Pizarro, D. Griffeath, D. Noguera, Quantitative cellular automaton model for biofilms, J. Environ. Eng. 127 (9) (1999) 782–789.
[16] C. Picioreanu, J.U. Kreft, M.C. van Loosdrecht, Particle-based multidimensional multispecies biofilm model, Appl. Environ. Microbiol. 70 (5) (2004) 3024–3040.
[17] O. Wanner, W. Gujer, A multispecies biofilm model, Biotechnol. Bioeng. XXVIII (1986) 314–328.
[18] E. Alpkvist, C. Picioreanu, M.C. van Loosdrecht, A. Heyden, Three-dimensional biofilm model with individual cells and continuum EPS matrix, Biotechnol. Bioeng. 94 (5) (2006) 961–979.
[19] N.G. Cogan, J.P. Keener, The role of the biofilm matrix in structural development, Math. Med. Biol. 21 (2) (2004) 147–166.
[20] T.R. Bott, M. Pinheiro, Biological fouling – velocity and temperature effects, Can. J. Chem. Eng. 55 (1977) 473–474.
[21] T. Else, C. Pantle, P. Amy, Boundaries for biofilm formation: humidity and temperature, Appl. Environ. Microbiol. 69 (8) (2003) 5006–5010.
[22] O. Wanner, A.B. Cunningham, R. Lundman, Modeling biofilm accumulation and mass transport in a porous medium under high substrate loading, Biotechnol. Bioeng. 47 (1995) 703–712.
[23] M.N. Ozisik, Boundary Value Problems of Heat Conduction, Dover, New York, 1989.
[24] K. Kajiwara, Y. Osada, Gels Handbook, Academic Press, 2000.
[25] A. Kumar, R.K. Gupta, Fundamentals of Polymers, McGraw-Hill, Ohio, 1997.
[26] P. Pavasant, L.M. Freitas dos Santos, E.N. Pistikopoulos, A.G. Livingston, Prediction of optimal thickness for membrane-attached biofilms growing in an extractive membrane bioreactor, Biotechnol. Bioeng. 52 (3) (1996) 373–386.
[27] A.A. Esener, J.A. Roels, N.W.F. Kossen, The influence of temperature on the maximum specific growth rate of klebsiella pneumoniae, Biotechnol. Bioeng. 23 (1981) 1401–1405.